

## Article

# Numerical Analysis on the Flue Gas Temperature Maintenance System of a Solid Fuel-Fired Boiler Operating at Minimum Loads

Michalina Kurkus-Gruszecka \*, Piotr Krawczyk and Janusz Lewandowski

Institute of Heat Engineering, Faculty of Power and Aeronautical Engineering, Warsaw University of Technology, Nowowiejska 21/25, 00-665 Warsaw, Poland; piotr.krawczyk@pw.edu.pl (P.K.); janusz.lewandowski@pw.edu.pl (J.L.)

\* Correspondence: michalina.kurkus-gruszecka.dokt@pw.edu.pl; Tel.: +48-22-264-5299

**Abstract:** Currently, energy policy is associated with the increase in the share of renewable sources in systemic energy production. Due to this trend, coal-fired power units must increase their work flexibility. Adapting a coal power plant to work with a lower load often causes the issue of maintaining the temperature before the selective catalytic reduction (SCR) installation at a sufficiently high level. This paper presents a CFD analysis of the mixing area of two flue gas streams before the SCR installation with various methods for mixing flue gas streams. The novelty of the work is mixing the flue gas streams of different temperatures using a flap shape developed by the authors. A series of numerical simulations were performed to develop the location and method of introducing the higher temperature gas, obtaining a uniform distribution of the exhaust gas temperature. The simulation scheme was applied to a series of geometrical modifications of the boundary conditions. The tested solution using only a single, straight flap in the flue gas duct allows the amplitude to be reduced from 298 K to 144 K. As a result of the research, a mixing flap design was developed to reduce the initial temperature amplitude of the flue gas streams from 298 K to 43 K.

**Keywords:** flue gas bypass; flue gas mixing; flue gas temperature before SCR; low-load power boiler operation; power plant flexibility



**Citation:** Kurkus-Gruszecka, M.; Krawczyk, P.; Lewandowski, J. Numerical Analysis on the Flue Gas Temperature Maintenance System of a Solid Fuel-Fired Boiler Operating at Minimum Loads. *Energies* **2021**, *14*, 4420. <https://doi.org/10.3390/en14154420>

Academic Editor: Marcin Kamiński

Received: 26 June 2021  
Accepted: 19 July 2021  
Published: 22 July 2021

**Publisher's Note:** MDPI stays neutral with regard to jurisdictional claims in published maps and institutional affiliations.



**Copyright:** © 2021 by the authors. Licensee MDPI, Basel, Switzerland. This article is an open access article distributed under the terms and conditions of the Creative Commons Attribution (CC BY) license (<https://creativecommons.org/licenses/by/4.0/>).

## 1. Introduction

Due to the increasing number of renewable energy sources with a share in energy systems, research is being conducted on a large scale to increase conventional power plant flexibility [1]. This aspect was addressed in [2], where the authors analyzed increased flexibility in systems with a high share of renewable sources. In [3], the flexibility and economic aspects of power plant operation in new low-carbon systems were analyzed. Increasing the flexibility of coal-fired power plant operation by activities related to the regulation of the steam cycle are presented in [4]. In [5,6], the cooperation of conventional power plants was analyzed in terms of the power grid flexibility. The works mentioned here are broadly related to increasing the power range flexibility to lower the coal unit minimum load [7]. At present, most coal-fired unit operating power fits the range of 50–100% of nominal capacity. In case of a significant power increase in the system due to the power produced by units with priority, e.g., renewables, the currently running conventional power plants reduce their operation [8]. If the power supplied to the electricity network still exceeds the demand, some conventional units have to be shut down and prepared for restart [9]. Shutting down and restarting coal-fired units is economically inefficient, shortens the unit's lifetime, and causes increased emissions of harmful substances [7]. Therefore, research to reduce the minimum power block output to values below 50% of the nominal load increases their stable operation under current conditions.

At the same time, the emission standards, concerning mainly dust, sulfur oxides, and nitrogen oxides emissions, have recently been stringent [3]. Selective catalytic reduction

(SCR) technology is the most frequently used for reducing nitrogen oxides in coal-fired power boilers, as indicated in [10,11]. Such installations require operation in a specific flue gas temperature range [11], between 585 K and 670 K, depending on the catalyst type. The required range is also indicated in [12] (the authors analyzed the installation and its impact on the quality of flue gases), and [13] concerns the installation's operation optimization. The issue that arises relatively often during attempts to increase the boiler operation flexibility is the insufficiently high flue gas temperature before the SCR installation, which results in its incorrect operation. One of the solutions for a too low temperature before the SCR issue is to connect the higher temperature flue gas from another part of the boiler to the main flue gas stream before the SCR installation. In the solution mentioned above, the key is to effectively mix the flue gas streams at different temperatures to obtain a uniform flue gas temperature field before the installation. The routing of an additional duct for transporting hot exhaust gases requires the consideration of design possibilities. In many modernized coal boilers, the SCR systems were installed additionally, so it is necessary to introduce hot flue gases from the top of the duct. There is a high risk of not mixing the hot flue gas stream with the main, cooler stream in such a configuration. The solution presented in this paper in the form of an adequately profiled turbulizing flap enables effective mixing of exhaust gas streams with the introduction of hot exhaust gas from the top of the duct and obtaining a temperature field with appropriate uniformity before the SCR installation.

If the elements regulating the flue gas flow installation, e.g., control vanes or flaps, are planned in an existing boiler, a key parameter that should be considered is the flue gas pressure drop caused by the installed element, especially in boiler operation with high loads. Any additional pressure drop in the flue gas ducts increases the flue gas fans' power consumption, and in some cases, it can cause fan inefficiency. Increased power consumption also negatively affects the overall power unit efficiency. The technology developed by the authors makes it possible to regulate the pressure drop caused by the additional turbulence flap, with the possibility to fold the flap during the boiler operation with the nominal load. Thus, the impact of the device on the flue gas pressure drop is reduced to a minimum.

With the increasing availability of computational power, computational fluid dynamics (CFD) is increasingly being applied to the calculation of power boilers [14–18], characterized by relatively large calculation volumes and multiple physical and chemical phenomena. CFD methods are used in power boiler calculations for many purposes. In [15], the CFD method was used to optimize nitrogen oxide removal from exhaust gases. The temperature distribution in the boiler, validated by acoustic measurements, was modeled in [16]. In several studies, the main objective was to determine the flue gas flow character in the boiler. In [17], the influence of the NO<sub>x</sub> control installation on the flue gas flow in a boiler was examined. The authors of [18] investigated heat transfer by conduction and radiation from the flue gases to the evaporator and boiler superheaters. The flue gas and air mix flow through the power boiler was analyzed in [19]. In [20], the exhaust gas recirculation performance was determined. Many studies have used CFD methods to calculate the distribution, formation and reduction of nitrogen oxides [21]. Many works also model sub-systems of power boilers, such as SCR reactors [10,22] or dedusting systems. In [23], the mixing of the flue gas stream with primary air was modeled to increase the flue gas temperature before the SCR installation. However, the authors did not present the geometry of the mixing system. Despite many works on numerical modeling of power boilers, there is a lack of models in the literature concerning the mixing of flue gas streams with different temperatures on a large scale. As the flow is non-reactive, without heat exchange with the environment, and is single phase. In terms of the computational model complexity, this type of numerical analysis has been carried out and verified many times over recent years. Nevertheless, there are always limitations and risks inherent in the use of such a calculation method. Today, models of this degree of complexity often allow the elimination of experimental confirmation in industrial applications. In addition, the model has been validated for the current flue geometry.

This article presents the selected results of the calculations that led to developing the final turbulence flap concept. The novelty of the work is the development of a device allowing for effective mixing of the flue gas streams while maintaining the following criteria:

- The hot flue gas stream is introduced from the top. Introducing the stream of hot flue gases from the bottom is impossible in terms of the boiler structure.
- The developed flap does not cause a significant pressure drop of exhaust gases during operation (40–60% of the nominal boiler load).
- The flap design allows it to be folded during boiler operation at nominal load so as to not interfere with the boiler operation.
- The device's design must be relatively simple and reliable because it is exposed to many hours of operation in high-temperature conditions and exhaust gas dustiness.

The developed shape of the flap allows for the flue gas stream to be mixed and obtain a uniform temperature field. Based on the analysis of the available literature, it is the first solution developed to mix the flue gas streams in the channel of a coal-fired boiler while maintaining the above criteria.

## 2. Model Description

### 2.1. Investigated Duct Location in the Boiler

The numerical model includes the flue gas flow through the external duct located downstream of the main boiler flue to the SCR installation, including introducing hot flue gases from the bypass duct into the main flue gas stream. A representative geometry of an OP-650 class coal-fired power boiler was chosen for the study. The analyzed boiler unit schematic with the key components highlighted is shown in Figure 1: the boiler outline, the SCR installation and the section of pipeline analyzed in this paper placed directly upstream of the SCR installation. In Figure 1, the flue gas flow path is also marked with blue arrows. The analyzed duct section is symmetrically divided on two sides of the boiler, which is well illustrated by the axonometric view located in the upper left corner of Figure 1.

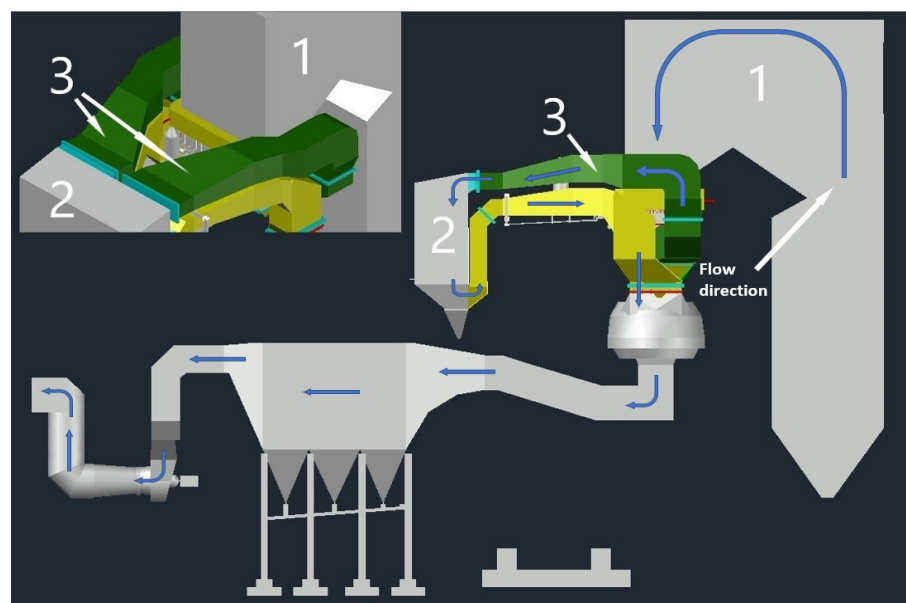


**Figure 1.** The analyzed boiler unit schematic with the key components: 1—boiler outline, 2—SCR installation, 3—analyzed duct section.

For further analyses, a section of the flue gas duct leading from the main boiler building to the SCR installation, marked in Figure 1 as number 3, was extracted from the presented geometry. As the analyzed duct section upstream of the SCR installation consists of two symmetrical parts, one of them was simulated in the numerical calculations using symmetry conditions.

## 2.2. The Developed Geometrical Variants

Four selected geometric options are presented in this paper, with the first three reflecting the progress of the fourth and final concept. As mentioned earlier, this study analyzed the bypass duct transporting higher temperature flue gases introduced from the top. The hot flue inlet configuration is the most difficult from the point of view of mixing the flue gas streams before the SCR system. The difficulty in mixing the flue gas streams is mainly due to buoyancy forces and relatively slow flue gas velocities resulting from low boiler load. To obtain a complete representation of the flue gas flow through the analyzed duct section, a full 3D geometry was implemented for the numerical calculations. A general schematic of the examined flue gas duct section is shown in Figure 2. The section shows the inlets of the flue gas streams and the flow direction towards the SCR reactor.

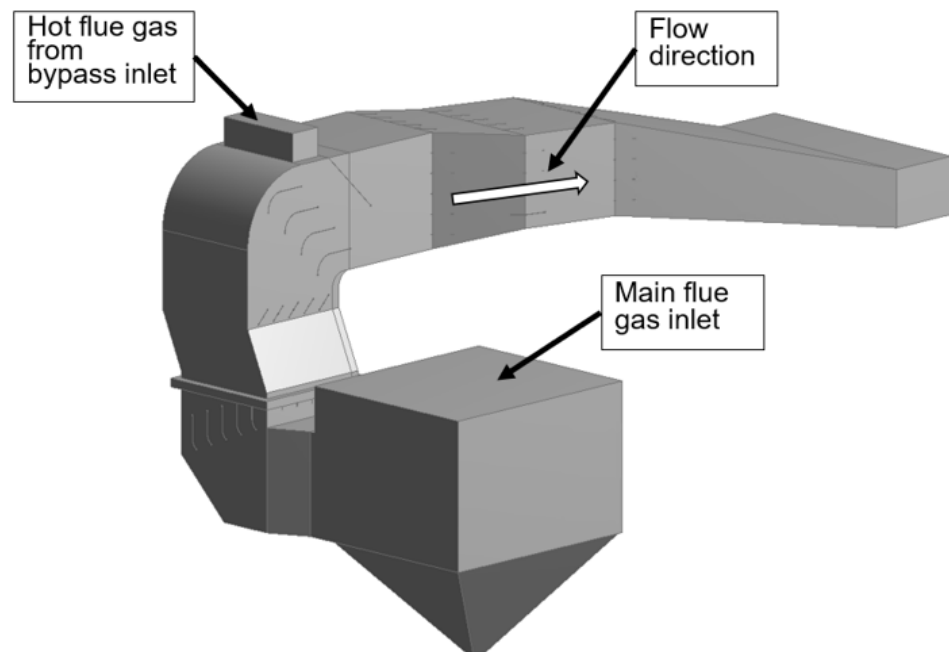


**Figure 2.** A general schematic of the examined flue gas duct section.

The geometric variants of the turbulence flap are shown in Figure 3. The geometries presented show the same bypass inlet location in each variant and the evolving geometry of the exhaust gas mixing elements. The other elements in the flue gas duct are fixed vanes which regulate the flue gas flow. The geometric variant G1 involves placing a single flap directly behind the hot flue gas inlet. The flap is inclined at an angle of 45 degrees and its length corresponds to covering half of the duct cross-section. A longer flap could not be used in this solution due to limitations on the maximum flue gas velocity, which increases as the flow cross-section area decreases.

In the geometric variant G2, three U-profiles were placed, with a total width of approximately two-thirds of the channel width and a length corresponding to covering half of the flow cross-section resulting from the velocity condition mentioned earlier. Geometric variations G3 and G4 are a combination of G1 and G2. They use a flat flap in the upper part and three U-profiles in the lower part. Both variants are constructed to cover half of the main duct cross-section. Variant G3 uses shorter but wider U-profiles with a total width of about the main duct of two-thirds. In variant G4, the profiles have a total width corresponding to half the main channel width. The designed geometries of the turbulence flaps, as seen from above, are shown in Figure 4.

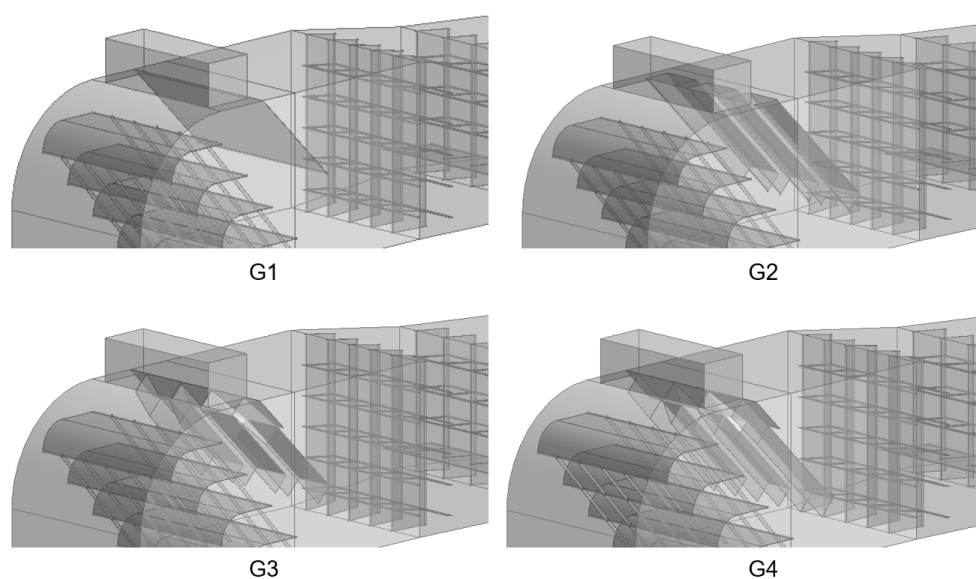


**Figure 3.** The four geometric variants developed, numbered from G1 to G4.

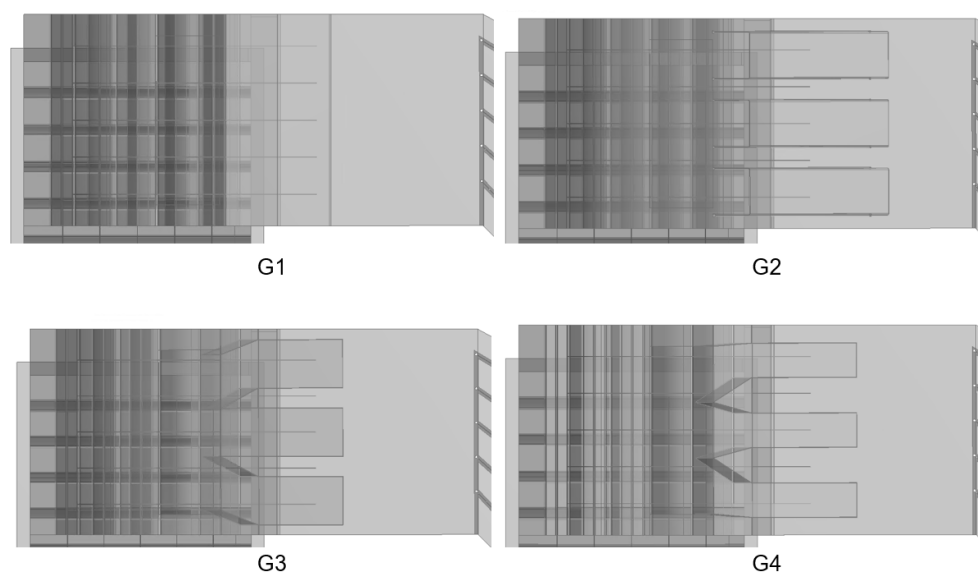


**Figure 4.** The four geometric variants seen from above, numbered from G1 to G4.

In order to adequately numerically reproduce the effects affecting the exhaust stream mixing, especially the buoyancy forces, the computational geometry was considered at a scale of 1:1. The basic geometrical dimensions of the analyzed channel section are shown in Table 1.

**Table 1.** The basic geometrical dimensions of the analyzed channel section.

Parameter	Value	Unit
Length of the analyzed channel section	32.10	m
Width of the analyzed channel section	17.35	m
Height of the analyzed channel section	18.13	m
Volume of the analyzed channel section	1094.5	m <sup>3</sup>

### 2.3. Flow-Governing Equations and Model Assumptions

The main equations of fluid mechanics applied to numerical calculations of gas flow such as momentum, mass, energy and species conservation were used for the calculations.

They are widely described in many works, e.g., in [24]. Momentum conservation is represented by Equation (1):

$$\frac{\partial}{\partial x_i}(\rho u_i u_j) + \frac{\partial P}{\partial x_j} = \frac{\partial}{\partial x_i} \left\{ \mu \left[ \frac{\partial u_j}{\partial x_i} + \frac{\partial u_i}{\partial x_j} - \frac{2}{3} \delta_{ij} \frac{\partial u_i}{\partial x_i} \right] \right\} + \frac{\partial}{\partial x_i}(-\rho u_j u_i) - F_p, \quad (1)$$

Mass conservation (Equation (2)) is presented below:

$$\frac{\partial}{\partial x_i}(\rho u_i) = \sum_J S_j, \quad (2)$$

Equation (3) represents conservation of energy:

$$\frac{\partial}{\partial x_i}(u_i[\rho E + P]) = \frac{\partial}{\partial x_j} \left( \lambda_{eff} \frac{\partial T}{\partial x_j} \right) + S_j, \quad (3)$$

The species conservation is given by Equation (4):

$$\frac{\partial}{\partial x_i}(\rho u_j Y_k) = - \frac{\partial}{\partial x_j} \vec{J}_k + \dot{\omega}_k + S_k, \quad (4)$$

A realizable k- $\epsilon$  turbulence model was implemented for the calculations, with full buoyancy forces included. Detailed descriptions of the above equations and the k-epsilon turbulence model with experimental verification are presented in [24]. The k- $\epsilon$  realizable model was implemented since it is widely used to calculate free gas flows in relatively large domains, such as in power boilers [19,20]. In [25], this model was used to develop a flow in a large-scale coal-fired boiler. The analyzed channel geometry includes elements that can cause rotation, wall boundary layers and gas recirculation. According to [26], the applied turbulence model can provide improved numerical simulation results in the abovementioned phenomena. In the k-epsilon model, Reynolds stresses are supplemented by the Boussinesq relation according to Equation (5):

$$-\rho u_j u_i = \mu_t \left( \frac{\partial u_i}{\partial x_j} + \frac{\partial u_j}{\partial x_i} \right) - \frac{2}{3} \left( \rho k + \mu_t \frac{\partial u_k}{\partial x_k} \right) \delta_{ij}, \quad (5)$$

With the turbulent viscosity calculated from Equation (6):

$$\mu_t = \rho C_\mu k^2 / \epsilon, \quad (6)$$

Unlike the standard and RNG models, the value of  $C_\mu$  is not constant in the k-epsilon realizable model.  $C_\mu$  is a function of the mean strain and rotation velocities and the turbulence fields represented by k and epsilon. The effective thermal conductivity can be calculated from the following formula (Equation (7)):

$$\lambda_{eff} = \lambda + c_P \mu_t / Pr_t, \quad (7)$$

Based on the literature [27], the turbulent Prandtl number was assumed to be 0.85.

In keeping with the character of the flue gas flow passing through the duct in an industrial power boiler, the model adopts the simplifications and basic assumptions outlined below:

- Compressible single-phase gas flow;
- As there are particulate settlers in the boiler, the existence of fly ash particles is ignored;
- Gravity field is included with full buoyancy effects;
- The radiation effect is neglected;
- Flue gas composition assumed as a result of coal combustion with a relatively high calorific value.

The discrete form of the equations above and all assumptions were implemented in ANSYS Fluent (18.2, ANSYS, Inc., Canonsburg, PA, USA).

#### 2.4. Meshes

As a full-scale 3D channel section simulation was analyzed, considering many elements installed in the channel, such as vanes and a turbulence flap, which require adequate calculation accuracy, so the implemented mesh is relatively large. The work performed a grid sensitivity analysis, examining grids with the following estimated number of elements:  $5.5 \times 10^6$ ,  $11 \times 10^6$ ,  $17.3 \times 10^6$ ,  $29 \times 10^6$ ,  $46 \times 10^6$ . The grid element count varies slightly between the analyzed cases, which is a direct result of the different turbulence flap geometries. In investigating the mesh sensitivity, several numerical simulations were performed analyzing parameters such as the final residual sum, mass, energy balance, maximum and minimum temperatures in the domain and pressure drop in the channel. The most reliable results were obtained for grids with 17.3, 29 and 46 million elements. Meshes with approximately 29 million elements were selected for further analysis because the parameters analyzed were highly reliable. The differences between the values obtained in the simulation with the 46 million grid did not exceed 1%. The chosen computational grid is shown in Figure 5.

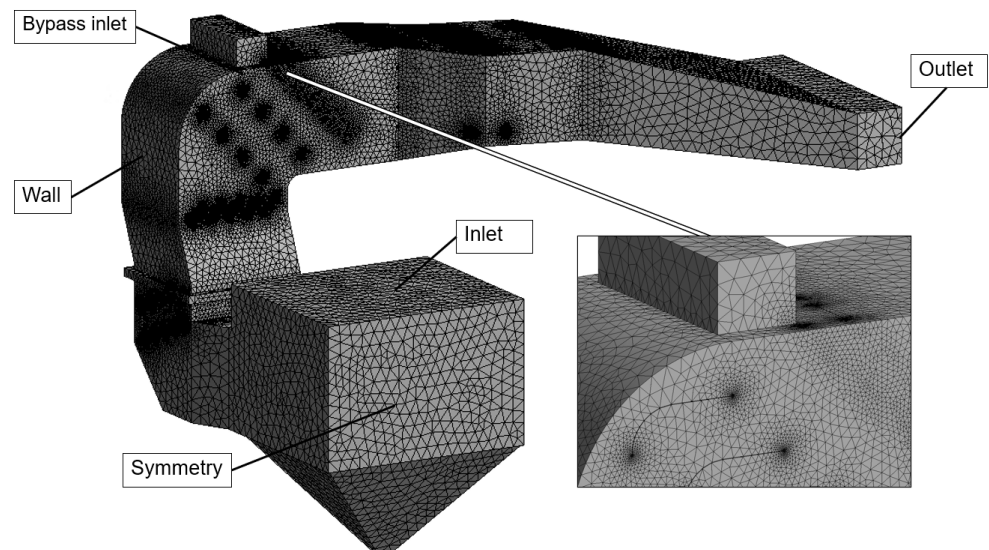


**Figure 5.** Computational grid of geometry G2 with a zoomed-in view and named selection marked.

As previously mentioned, the analyzed channel section contains many installed irregular-shaped flow control elements that significantly influence the simulation results. Therefore, an unstructured mesh was used in the computational domain, introducing the necessity of using more computing power. The mesh was given appropriately named selections corresponding to the boundary conditions described in the following subsection. The named regions are also shown in Figure 5.

#### 2.5. Boundary Conditions and Simulations Settings

Each of the computational domains corresponding to the geometric variants was given homogeneous boundary conditions. The zones defined are inlet, bypass inlet, outlet, wall and symmetry, marked in Figure 5. The inlet boundary condition corresponds to a flow of 90% of the main exhaust stream at a temperature lower than that required for the efficient operation of the SCR reactor. The design inlet type was defined as a mass flow inlet. The main inlet turbulence was specified with the intensity ratio and the hydraulic diameter. Immediately upstream of the design inlet, the boiler has a heat exchanger covering the entire cross-section of the flue gas duct. Therefore, the flue gas flow upstream of the inlet is

relatively uniform and regulated, making it possible to apply the uniform velocity field condition at the domain inlet.

The bypass inlet boundary condition corresponds to the higher temperature flue gases introduced into the main duct. These flue gases are led at 10% of the total amount from the higher temperature boiler part. Mixed with 90% of the flue gases from the main duct, they are supposed to ensure the safe operation of the SCR reactor in the appropriate temperature range. The design type of the bypass flue gas inlet is a mass flow inlet type with a uniform perpendicular velocity field. The uniform velocity field simplification was applied due to the relatively large dimensions of the duct, whose cross-section is almost four square meters. The flow is not laminar, and wall effects are negligible. The turbulence was specified with the intensity ratio and the inlet bypass duct hydraulic diameter.

The domain outlet located just upstream of the SCR reactor was defined as a pressure outlet. The appropriate conditions were applied, such as backflow temperature, exhaust composition and turbulence defined by the intensity and hydraulic outlet diameter.

The remaining boundary conditions are the symmetry condition and the wall condition. The symmetry condition was given on one surface, indicated in Figure 5, and it corresponds to the second, symmetrical part of the boiler, clearly visible in Figure 1. The wall condition was given on all other surfaces of the computational domain, i.e., the external surfaces of the duct as well as all surfaces corresponding to the flow control elements installed in the duct. All walls both inside and outside the channel were modeled as adiabatic. This approach was justified because the walls inside the duct, which are part of the flow control elements, are heated up to the temperature of the flue gases during the continuous boiler operation. Meanwhile, the external duct walls are well insulated, as indicated by modern temperature measurements installed within the examined boiler section.

The key chemical reactions affecting the flue gas composition no longer occur within the investigated boiler section, so the composition was assumed to be homogeneous for the inlets and the outlet. The flue gas composition and other boundary conditions are shown in Table 2. As symmetrical duct operation was simulated, the mass values refer to half of the flow.

**Table 2.** Flue gas composition and the main boundary conditions.

Parameter	Value	Unit
Oxygen volume fraction in the flue gas	0.033	-
Carbon dioxide volume fraction in the flue gas	0.137	-
Water vapor volume fraction in the flue gas	0.080	-
Nitrogen volume fraction in the flue gas	0.739	-
Other triatomic gas volume fraction in the flue gas	0.010	-
Main flow inlet temperature	567	K
Bypass inlet temperature	867	K
Outlet backflow temperature	597	K
Main inlet flow mass share	90	%
Bypass flow mass share	10	%
Main inlet mass flow	53.5473	kg/s
Bypass inlet mass flow	5.9497	kg/s

The key applied solver settings in ANSYS Fluent are coupled scheme with second order discretization for all parameters, pseudo-transient mode, convergence criteria: 10<sup>-4</sup>. In order to properly evaluate the simulation correctness, relevant parameters were monitored: outlet mass flow, mass-weighted outlet temperature, maximum and minimum temperature in the domain, pressure drop across the duct. The accuracy of the monitored parameters was obtained at a level below 0.1%. Simulations were carried out with a computing server and utilization of 60 cores. The time required to run a single simulation was approximately 8 h.

The numerical model was verified by comparing the current boiler geometry modeling results with the empirical values. The calculations were performed for several operational

states of the boiler. The obtained results of temperatures, pressure drops and exhaust gas velocity distribution were compared with the current measurement data. The parameters calculated using the numerical model for the existing boiler structure were convergent with the measured parameters.

### 3. Results and Discussion

After calculating all geometric variants, and checking the results for correctness through appropriate monitors, the outcomes obtained were evaluated. The most important results testifying the effectiveness of mixing flue gas streams with different temperatures are the temperature fields generated by the calculations carried out. The flue gas temperature distribution for each geometric variant in the plane intersecting the design domain is shown in Figure 6. The right-hand side of Figure 6 also shows the temperature distribution on a plane perpendicular to the direction of flow, intersecting the mixing flap.

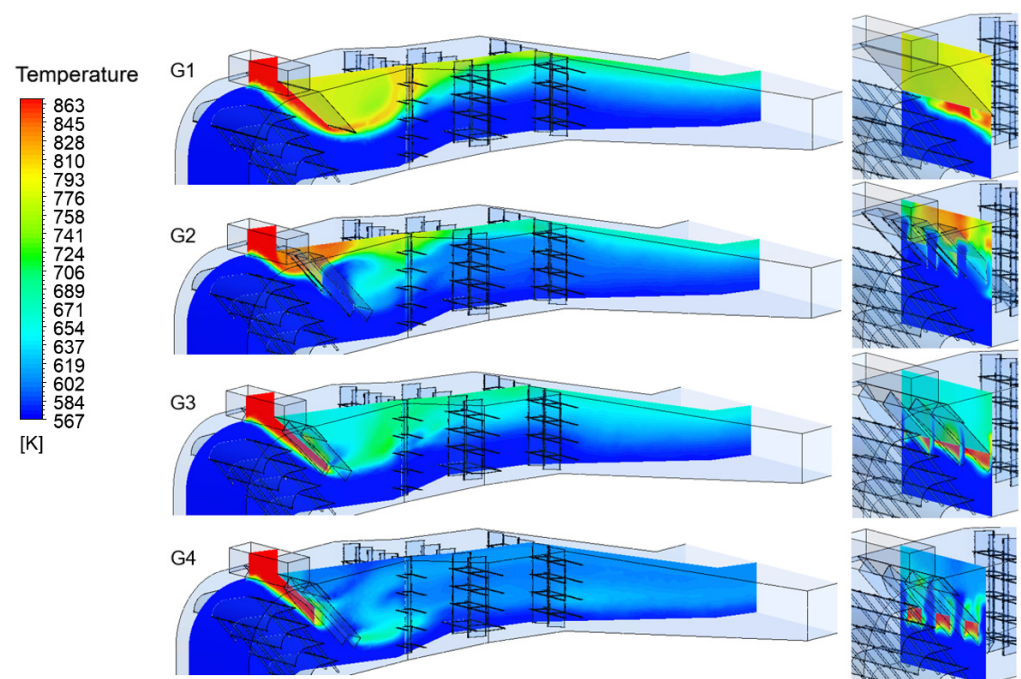


**Figure 6.** The flue gas temperature distribution for each geometric variant in the plane intersecting the computational domain (on the left) and in the plane perpendicular to the flow direction intersecting the mixing flap (on the right).

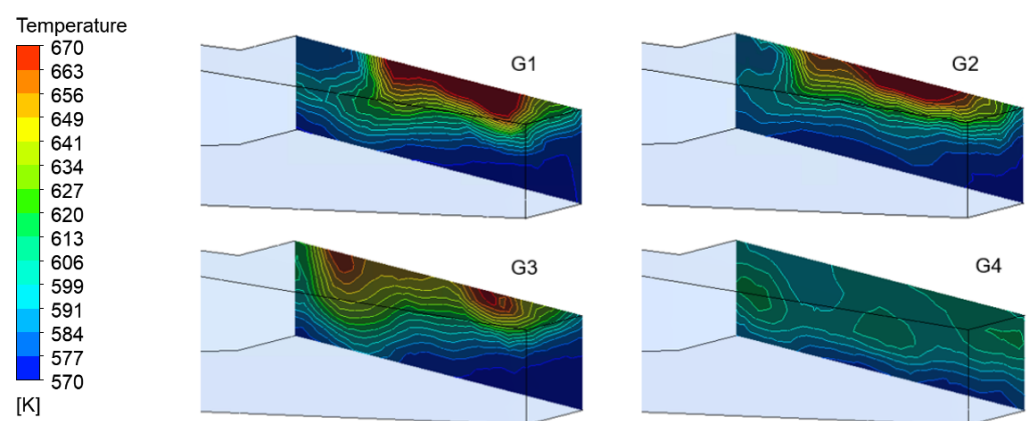
After analyzing the simulation results, it can be concluded that the most uniform temperature distribution was obtained for the G4 geometric variant. The simulation results of G1 variant indicate that the higher temperature exhaust gas is initially led to the lower part of the duct. However, immediately after the mixing flap, through buoyancy forces and the mass-dominant flow of the denser exhaust gas with a lower temperature, the hot exhaust gas is pushed to the upper part of the duct. They are then mixed to a small extent in the further duct section.

In variant G2, where U-profiles are used, mixing the flue gases is slightly better than in variant G1. In that case, however, most of the hot flue gases right after the bypass duct inlet are forced by the stream of denser and cooler flue gases into the spaces between the U-profiles and flush out the hot flue gases from further parts of the U-profiles. Therefore, the U-profiles installed in this way do not fulfill their intended role, not delivering the hot flue gases to the lower main duct section. Immediately after the mixing flap, the flue gases are directed upwards by buoyancy forces and mix to a small extent in the further section of the duct.

Variant G3 shows an improvement in the level of flue gas mixing compared to variants G1 and G2. The application of U-profiles with a flat section at the flap top allows for an appropriate hot flue gas distribution to the lower parts of the U-profiles. The initial flat section prevents hot flue gases from being washed out by the lower temperature main stream. However, as previously mentioned, the dimensions of each flap had to be adapted to the condition of maximum coverage of half the main duct cross-section. Therefore, U-profiles with a total width of two-thirds the width of the duct cannot be longer. Since the U-profile of variant G3 is wide but relatively short, the hot flue gases are not introduced deep enough to mix effectively with the cold flue gases.

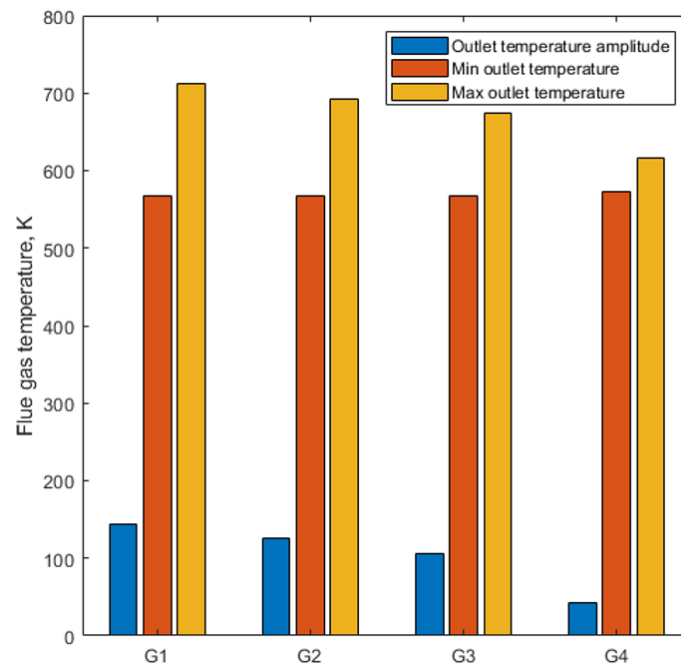
The G4 variant represents the final concept developed, which represents a modification of the G3 variant. Similar to variant G3, a flat section is used in the upper flap section followed by three U-profiles. Variant G4 uses U-profiles that are narrower and longer than the profiles used in variant G3. As with G3, the flat section of the flap prevents the hot flue gases from being washed out in the upper duct section and ensures adequate hot flue gas distribution to the U-profiles. Sufficiently long profiles transport the hot flue gases to the lower part of the main duct. Then, due to the buoyancy forces, the hot flue gases are mixed with the main flue gas stream of higher density and lower temperature. Further downstream, the flue gas temperature is homogenized. Since the plane on which the temperature is displayed follows the curvature of the flue gas duct, clearly visible in Figure 1, the hot flue gas portion in the U-profile is cut off, so the observer cannot see the hot flue gas entering the end of the profile.

Figure 7 shows the temperature distributions at the computational domain outlet, corresponding to the SCR reactor exhaust inlet. The temperature scale has been narrowed to 100 K (from 570 to 670 K). The target temperature of the perfectly mixed exhaust gas is 597 K. The best degree of mixing of flue gases was obtained in the geometrical variant G4, as can be seen in Figure 7. In this case, the maximum flue gas temperature was 616 K, which is only 2.18% of the percentage deviation from the perfectly mixed flue gas temperature of 597 K. The minimum flue gas temperature, in this case, was 573.6, which is a deviation of 3.91% from the target temperature. In the cases G1–G3, the temperature amplitudes are considerably larger. All exceed values of 100 K. Simultaneously, in the lower section of the duct, flue gases with a low temperature (close to the initial temperature of the main stream) are observed, which indicates a complete lack of mixing of the lower layers of flue gases.



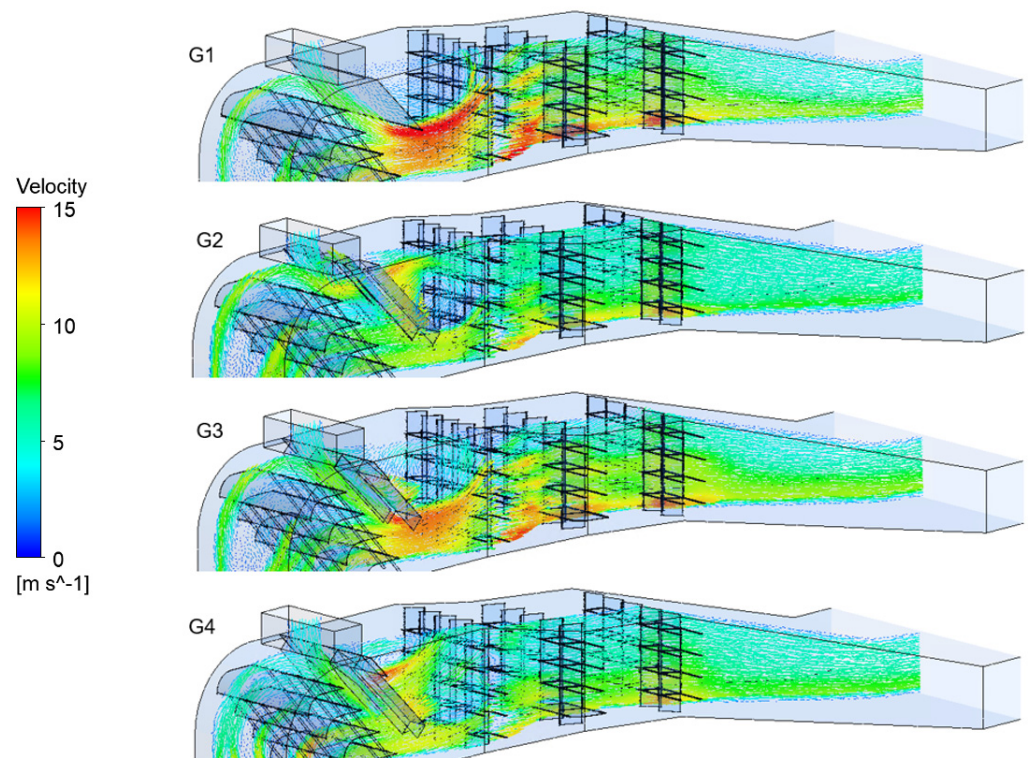
**Figure 7.** The temperature distributions at the computational domain outlet for each geometric variant.

Figure 8 shows a plot of the minimum and maximum temperatures found for each geometric variant at the outlet of the computational domain representing the inlet to the SCR reactor. The graph also shows the temperature amplitudes at the domain outlet, indicating the degree of exhaust gas stream mixing.



**Figure 8.** Plot of temperature and amplitude of flue gas temperature at duct outlet for each geometric variant.

The velocity vectors determined on the plane intersecting the computational domain are shown in Figure 9. It can be seen that for variant G1, the velocity of the main flue gas stream increases significantly in the area under the turbulizing flap. Meanwhile, a low-pressure field and backflows are created in the upper part behind the flap. In the G2 variant, the flue gases flow freely through the spaces between the turbulence flap's U-profiles, creating a slight swirl of gas behind the flap. The flow is then stabilized. As in the geometrical variant G1, in the variant G3 with its wide U-profile, the main exhaust flow velocity increases significantly in the area below the flap. Above the flap, a low-pressure field is created together with the backflow. The most uniform velocity field was obtained for variant G4, which is also the most effective in mixing the exhaust gas streams. The main exhaust stream flows gently through the relatively wide spaces between the flap U-profiles. Slight turbulence is created in the upper duct behind the flat part of the turbulence flap.



**Figure 9.** The flue gas velocity distribution for each geometric variant in the plane intersecting the computational domain.

#### 4. Conclusions

This article presents an innovative method of mixing flue gas streams in a coal boiler using the designed mixing flap. The presented work is concerned with supporting the SCR system operation under low-load conditions of coal-fired boilers, contributing to the flexibility of the operation of these devices. The developed solution was exposed to CFD calculations, in which the distributions of temperature, velocity, density and other key thermodynamic parameters were examined. The results indicate that the invented flap works as intended, causing an adequate mixing of the exhaust gas streams. It results in a uniform gas temperature field before the inlet to the SCR system. The analyses showed that the mixing flap developed by the authors could lower the flue gas amplitude in the desired cross-section from 298 K to 43 K. In the intermediate solutions, amplitudes of 144, 125 and 106 K were obtained. By appropriate mixing, the maximum flue gas temperature was reduced by 251 K. In addition, the developed solution was subjected to computational analyses with regard to its functioning in the case of boiler operation with nominal load. The flap, as previously mentioned, can be folded towards the upper wall of the duct. It allows safe boiler operation in nominal conditions without significant pressure losses in the flue gas duct.

The developed solution entails investment costs and operating costs. However, due to the current energy policy and the need for coexistence of coal-fired boilers with renewable energy sources, such solutions are necessary for these facilities to function. As in the flue gas treatment installation, this type of modernization does not provide direct profits from the implementation but allows the facility to operate in new conditions of the energy system.

It is planned to create a construction design and then install the device on the OP-650 boiler in the longer term. Work will then be carried out to optimize the method. The next steps will involve the application of the method in coal boilers with different power ranges. Although the solution is dedicated to power boilers, it is possible to use the developed concept in other systems requiring mixing gases with different temperatures.

**Author Contributions:** Conceptualization, P.K., M.K.-G. and J.L.; final geometrical concept, P.K.; methodology, P.K. and M.K.-G.; numerical simulation, M.K.-G.; writing—original draft preparation, M.K.-G.; writing—review and editing, M.K.-G.; visualization, M.K.-G.; supervision, P.K. and J.L.; project administration, P.K. and J.L. All authors have read and agreed to the published version of the manuscript.

**Funding:** This research received no external funding.

**Acknowledgments:** This research is supported by the National Centre for Research and Development which is co-financed by the European Union in the framework of the Smart Growth Operational Programme and the Power Units 200+ Program. Innovative technology of changing the operating regime of 200 MWe power units.

**Conflicts of Interest:** The authors declare no conflict of interest.

## Nomenclature

$c_p$	specific heat, J/(kg K)
$E$	fluid total energy, J/kg
$F_p$	pressure force, N
$J$	species mass fluxes, kg/s
$k$	turbulence kinetic energy, J/kg
$P$	fluid static pressure, Pa
$S$	mass source term, kg/(m <sup>3</sup> s)
$S_h$	energy source term, W/m <sup>3</sup>
$T$	temperature, K
$u$	velocity, m/s
$x$	tensor length, m
$Y$	species mass fraction
Greek symbols	
$\varepsilon$	turbulent kinetic energy dissipation rate
$\dot{\omega}$	species production/destruction rate, kg/(m <sup>3</sup> s)
$\rho$	gas density, kg/m <sup>3</sup>
$\lambda$	thermal conductivity, W/(m K)
$\delta$	the Kronecker delta,
$\mu$	viscosity, Pa s
Subscripts and superscripts	
$eff$	effective
$i$	tensor direction
$j$	tensor direction
$k$	species index
$t$	turbulent

## References

1. Yoshiba, F.; Hanai, Y.; Watanabe, I.; Shirai, H. Methodology to evaluate contribution of thermal power plant flexibility to power system stability when increasing share of renewable energies: Classification and additional fuel cost of flexible operation. *Fuel* **2021**, *292*, 120352. [\[CrossRef\]](#)
2. Kubik, M.L.; Coker, P.J.; Barlow, J.F. Increasing thermal plant flexibility in a high renewables power system. *Appl. Energy* **2015**, *154*, 102–111. [\[CrossRef\]](#)
3. Brouwer, A.S.; van den Broek, M.; Seebregts, A.; Faaij, A. Operational flexibility and economics of power plants in future low-carbon power systems. *Appl. Energy* **2015**, *156*, 107–128. [\[CrossRef\]](#)
4. Zhao, Y.; Wang, C.; Liu, M.; Chong, D.; Yan, J. Improving operational flexibility by regulating extraction steam of high-pressure heaters on a 660 MW supercritical coal-fired power plant: A dynamic simulation. *Appl. Energy* **2018**, *212*, 1295–1309. [\[CrossRef\]](#)
5. Motalleb, M.; Thornton, M.; Reihani, E.; Ghorbani, R. Providing frequency regulation reserve services using demand response scheduling. *Energy Convers. Manag.* **2016**, *124*, 439–452. [\[CrossRef\]](#)
6. Denholm, P.; Hand, M. Grid flexibility and storage required to achieve very high penetration of variable renewable electricity. *Energy Policy* **2011**, *39*, 1817–1830. [\[CrossRef\]](#)
7. Oree, V.; Sayed Hassen, S.Z. A composite metric for assessing flexibility available in conventional generators of power systems. *Appl. Energy* **2016**, *177*, 683–691. [\[CrossRef\]](#)

8. Ulbig, A.; Andersson, G. Analyzing operational flexibility of electric power systems. *Int. J. Electr. Power Energy Syst.* **2015**, *72*, 155–164. [[CrossRef](#)]
9. Alizadeh, M.I.; Parsa Moghaddam, M.; Amjady, N.; Siano, P.; Sheikh-El-Eslami, M.K. Flexibility in future power systems with high renewable penetration: A review. *Renew. Sustain. Energy Rev.* **2016**, *57*, 1186–1193. [[CrossRef](#)]
10. Liu, X.; Tan, H.; Wang, Y.; Yang, F.; Mikulčić, H.; Vujanović, M.; Duić, N. Low NO<sub>x</sub> combustion and SCR flow field optimization in a low volatile coal fired boiler. *J. Environ. Manag.* **2018**, *220*, 30–35. [[CrossRef](#)]
11. Xiang, J.; Wang, P.; Su, S.; Zhang, L.; Cao, F.; Sun, Z.; Xiao, X.; Sun, L.; Hu, S. Control of NO and Hg<sub>0</sub> emissions by SCR catalysts from coal-fired boiler. *Fuel Process. Technol.* **2015**, *135*, 168–173. [[CrossRef](#)]
12. Li, Z.; Jiang, J.; Ma, Z.; Wang, S.; Duan, L. Effect of selective catalytic reduction (SCR) on fine particle emission from two coal-fired power plants in China. *Atmos. Environ.* **2015**, *120*, 227–233. [[CrossRef](#)]
13. Pritchard, S.; DiFrancesco, C.; Kaneko, S.; Kobayashi, N.; Suyama, K.; Iida, K. Optimizing SCR Catalyst Design and Performance for Coal-Fired Boilers. In Proceedings of the EPRI/EPA 1995 Joint Symposium on Stationary Combustion, Kansas City, MO, USA, 16–19 May 1995.
14. Dal Secco, S.; Juan, O.; Louis-Louisy, M.; Lucas, J.Y.; Plion, P.; Porcheron, L. Using a genetic algorithm and CFD to identify low NO<sub>x</sub> configurations in an industrial boiler. *Fuel* **2015**, *158*, 672–683. [[CrossRef](#)]
15. Modliński, N.; Madejski, P.; Janda, T.; Szczepanek, K.; Kordylewski, W. A validation of computational fluid dynamics temperature distribution prediction in a pulverized coal boiler with acoustic temperature measurement. *Energy* **2015**, *92*, 77–86. [[CrossRef](#)]
16. Adamczyk, W.P.; Isaac, B.; Parra-Alvarez, J.; Smith, S.T.; Harris, D.; Thornock, J.N.; Zhou, M.; Smith, P.J.; Żmuda, R. Application of LES-CFD for predicting pulverized-coal working conditions after installation of NO<sub>x</sub> control system. *Energy* **2018**, *160*, 693–709. [[CrossRef](#)]
17. Madejski, P. Numerical study of a large-scale pulverized coal-fired boiler operation using CFD modeling based on the probability density function method. *Appl. Therm. Eng.* **2018**, *145*, 352–363. [[CrossRef](#)]
18. Laubscher, R.; Rousseau, P. CFD study of pulverized coal-fired boiler evaporator and radiant superheaters at varying loads. *Appl. Therm. Eng.* **2019**, *160*, 114057. [[CrossRef](#)]
19. Rajh, B.; Yin, C.; Samec, N.; Hriberšek, M.; Kokalj, F.; Zadravec, M. Advanced CFD modelling of air and recycled flue gas staging in a waste wood-fired grate boiler for higher combustion efficiency and greater environmental benefits. *J. Environ. Manag.* **2018**, *218*, 200–208. [[CrossRef](#)] [[PubMed](#)]
20. Gómez, M.A.; Martín, R.; Chapela, S.; Porteiro, J. Steady CFD combustion modeling for biomass boilers: An application to the study of the exhaust gas recirculation performance. *Energy Convers. Manag.* **2019**, *179*, 91–103. [[CrossRef](#)]
21. Kurkus-Gruszecka, M.; Krawczyk, P.; Badyda, K. Wpływ wybranych parametrów operacyjnych lancy wtryskowej na dystrybucję reagenta w komorze paleniskowej kotła energetycznego. *Rynek Energii* **2019**, *144*, 46–51.
22. Zeng, H.; Yuan, J.; Wang, J. Optimal design of a tower type SCR-deNO<sub>x</sub> facility for a 1000 MW coal-fired power plant based on CFD simulation and FMT validation. *Appl. Sci.* **2019**, *9*, 1012. [[CrossRef](#)]
23. Wang, G.; Zhang, L.; Ai, D.; Zhao, Y.; Zhou, Y. Research on No<sub>x</sub> Formation and SCR Denitration System Control by Smoke Mixing under Low Load. *IOP Conf. Ser. Earth Environ. Sci.* **2020**, *440*, 042053. [[CrossRef](#)]
24. Shih, T.-H.; Liou, W.W.; Shabbir, A.; Yang, Z.; Zhu, J. A New k-ε Eddy Viscosity Model for High Reynolds Number Turbulent Flows. *Comput. Fluids* **1995**, *24*, 227–238. [[CrossRef](#)]
25. Xu, Y.; Zhang, Y.; Liu, F.; Shi, W.; Yuan, J. CFD analysis on the catalyst layer breakage failure of an SCR-DeNO<sub>x</sub> system for a 350 MW coal-fired power plant. *Comput. Chem. Eng.* **2014**, *69*, 119–127. [[CrossRef](#)]
26. ANSYS ANSYS FLUENT Theory Guide. *Knowl. Creat. Diffus. Util.* **2010**, *15317*, 724–746.
27. Weigand, B.; Ferguson, J.R.; Crawford, M.E. An extended Kays and Crawford turbulent Prandtl number model. *Int. J. Heat Mass Transf.* **1997**, *40*, 4191–4196. [[CrossRef](#)]